
Joint Representations for Reinforcement Learning with Multiple Sensors

Philipp Becker*

Karlsruhe Institute of Technology

Sebastian Markgraf

Karlsruhe Institute of Technology

Fabian Otto

Bosch Center for Artificial Intelligence
University of Tübingen

Gerhard Neumann

Karlsruhe Institute of Technology

Abstract

Combining inputs from multiple sensor modalities effectively in reinforcement learning (RL) is an open problem. While many self-supervised representation learning approaches exist to improve performance and sample complexity for image-based RL, they usually neglect other available information, such as robot proprioception. However, using this proprioception for representation learning can help algorithms to focus on relevant aspects and guide them toward finding better representations. In this work, we systematically analyze representation learning for RL from multiple sensors by building on *Recurrent State Space Models*. We propose a combination of reconstruction-based and contrastive losses, which allows us to choose the most appropriate method for each sensor modality. We demonstrate the benefits of joint representations, particularly with distinct loss functions for each modality, for model-free and model-based RL on complex tasks. Those include tasks where the images contain distractions or occlusions and a new locomotion suite. We show that combining reconstruction-based and contrastive losses for joint representation learning improves performance significantly compared to a post hoc combination of image representations and proprioception and can also improve the quality of learned models for model-based RL.

1 Introduction

Learning compact representations of high-dimensional images has led to considerable advances in reinforcement learning (RL) from pixels. To date, most RL approaches that use representations [14, 15, 44, 23, 56, 46, 59], learn them in isolation for a single high-dimensional sensor, such as a camera. However, while images are crucial to the perception of an agent’s surroundings in unstructured environments, they are often not the only source of information available. Most agents in realistic scenarios can also directly observe their internal state using sensors in their actuators, inertial measurement units, force and torque sensors, or other forms of proprioceptive sensing.

State Space Models [28] naturally lend themselves to accumulating information across multiple sensors and time to form a single compact representation of the entire system state. By building on *Recurrent State Space Models (RSSMs)* [14], this approach provides a scalable basis for RL in tasks with complex observations and dynamics.

Previous work suggests using either reconstruction [14, 16] or contrastive methods [15, 25, 30] to train *RSSMs*, both of which have their strengths and weaknesses. While reconstruction is a powerful tool as it forces models to capture the entire signal, it may fail to learn good representations if

*Correspondence to philipp.becker@kit.edu

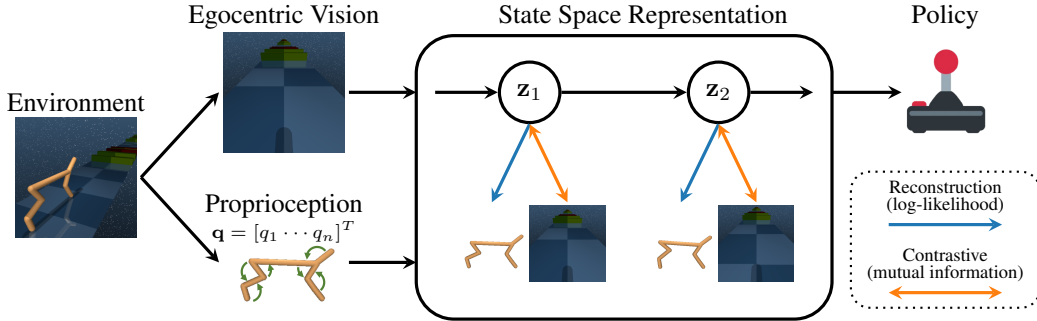


Figure 1: For many reinforcement learning problems, more than one sensor modality is available. For example, in the shown task from our *Locomotion Suite*, the robot has an egocentric vision to perceive the obstacles in its environment and observes its proprioceptive state, i. e., the position and velocity of its body parts. We propose learning a joint representation of all available sensor sources using a combination of reconstruction-based and contrastive objectives. This approach allows us to use reconstruction for clean low-dimensional sensors, e.g., proprioception, and contrastive losses for high-dimensional noisy sensor signals such as images. We build on *Recurrent State Space Models* to accumulate information across sensors and time and use our representations for model-free and model-based RL.

observations are noisy or contain distracting elements [59, 25, 7]. In such cases, contrastive methods can ignore irrelevant parts of the observation and still learn valuable representations. However, they are prone to representation collapse and can struggle to learn accurate dynamics models required for model-based RL [25].

We propose combining contrastive and reconstruction-based approaches to leverage the benefits of both worlds. For example, reconstruction-based loss functions can be used for noiseless proprioception and a contrastive loss for images with distractors, where reconstruction fails [25, 30]. Figure 1 shows an overview of this approach. The common approach to training *RSSMs* is variational inference (VI), which provides a basis for both reconstruction and contrastive objectives. In the original formulation [14], *RSSMs* are trained with VI using pure reconstruction. However, the reconstruction terms can be replaced with contrastive losses based on mutual information estimation [15, 25]. Contrastive predictive coding (CPC) [33] offers an alternative to the variational approach of training *RSSMs* [30, 45]. These methods train the *RSSMs*' system dynamics by maximizing the agreement of predicted future latent states with future observations. Since the recent literature is inconclusive about whether the variational or the predictive approach is preferable, we evaluate our representation learning using both methods. We build our representation learning method into model-free and model-based RL agents and systematically evaluate the effects of learning a joint representation on tasks from the DeepMind Control (DMC) Suite [47]. To test the ability of all approaches to cope with distractions and incomplete information, we use modified DMC Suite tasks to use natural video backgrounds [59, 30] and occlusions. Furthermore, we evaluate the methods on a new locomotion suite where agents must combine proprioception and egocentric vision to move and navigate.

Our experiments show that joint representations improve performance over learning an image-only representation and concatenating it with proprioception. They allow us to solve tasks with distractors and occlusions. In particular, the latter task is out of reach for pure image representations. Moreover, we show that joint representations improve the performance of model-based agents with contrastive image representations, which are known to perform worse than reconstruction-based approaches [15, 25]. Here, on the task with natural background, using a combination of reconstruction and contrastive losses enables us to perform almost as well as pure reconstruction on noise-free images.

To summarize our contributions, we propose a general framework for training joint representations based on *RSSMs* by combining contrastive and reconstruction losses based on the properties of the individual sensor modalities. This framework contains objectives motivated by a variational and a contrastive predictive coding viewpoint. We conduct a large-scale evaluation using model-free and model-based approaches and show that using joint representations significantly increases performance over concatenating image representations and proprioception. Further, they help to learn better models for model-based RL when a contrastive image loss is required. We introduce DMC control suite tasks

with occlusions and a locomotion suite as new challenges for representation learning in RL. Our joint representation approach outperforms several SOTA baselines on these challenging tasks and on tasks with natural video backgrounds and allows solving tasks where image-only approaches fail.

2 Related Work

Representations for Reinforcement Learning. Many recent approaches use ideas from generative [50, 52, 3, 23, 56] and self-supervised representation learning [59, 44, 55, 46, 58] to improve performance, sample efficiency, and generalization of RL from images. Particularly relevant for this work are those based on *Recurrent State Space Models (RSSMs)*. When proposing the *RSSM*, [14] used a generative approach. They formulated their objective as auto-encoding variational inference, which trains the representation by reconstructing observations. Such reconstruction-based approaches have limitations with observations containing noise or many task-irrelevant details. As a remedy, [15] proposed a contrastive alternative based on mutual information and the InfoNCE estimator [35]. [25] refined this approach and improved results by modifying the policy learning mechanism. Using a different motivation, namely contrastive predictive coding [33], [31, 30, 45, 32] proposed alternative contrastive learning objectives for *RSSMs*. In this work, we leverage the variational and predictive coding paradigms and show that joint representations improve performance for both. [10, 51] propose further factorizing the *RSSM*'s latent variable to disentangle task-relevant and task-irrelevant information. However, unlike contrastive approaches, they explicitly model the task-irrelevant parts instead of ignoring them, which can impede performance if the distracting elements become too complex to model. Other recent approaches for learning *RSSMs* include using prototypical representations [7] or masked reconstruction [39]. Out of these works, only [45] consider using additional proprioceptive information. Yet, they did so only in a single experiment, without comparing to the concatenation of image representations and proprioception or investigating a combination of reconstruction and contrastive losses.

Sensor Fusion in Reinforcement Learning. Many application-driven approaches to visual RL for robots use proprioception to solve their specific tasks [9, 24, 19, 54, 11]. Yet, they usually do not use dedicated representation learning or concatenate image representations and proprioception. Several notable exceptions use *RSSMs* with images and proprioception and thus learn joint representations [53, 17, 4, 18]. However, all of them focus on a purely model-based setting and do not investigate joint-representation learning with *RSSMs* as an alternative to concatenation for model-free RL. Additionally, they only consider reconstruction-based training objectives for joint representation learning, while we emphasize contrastive and especially combined methods.

Multimodal Representation Learning. Representation learning from multiple modalities has widespread applications in general machine learning, where methods such as *CLIP* [36] combine language concepts with the semantic knowledge of images and allow language-based image generation [37]. For robotics, [5, 27, 8, 40, 41] combine language models with the robot's perception for natural language-guided manipulation tasks using imitation learning. In contrast, we work in an online RL setting and mainly consider different modalities, namely images and proprioception.

3 Learning Representation from Multiple Sensors with State Space Models

Given trajectories of observations $\mathbf{o}_{1:T} = \{\mathbf{o}_t\}_{t=1:T}$ and actions $\mathbf{a}_{1:T} = \{\mathbf{a}_t\}_{t=1:T}$ we aim to learn a state representation that is well suited for RL. We assume the observations stem from K different sensor sources, $\mathbf{o}_t = \{\mathbf{o}_t^{(k)}\}_{k=1:K}$, where the individual $\mathbf{o}_t^{(k)}$ might be high dimensional, noisy, and contain only partial information about the system. Further, even the whole observation \mathbf{o}_t may not contain all the information necessary for acting optimally, i. e., the environment is partially observable, and the representation has to accumulate information over time to allow optimal acting.

Our goal is to learn a concise, low dimensional representation $\phi(\mathbf{o}_{1:t}, \mathbf{a}_{1:t-1})$ that accumulates all relevant information until time step t . We provide this representation to a policy $\pi(\mathbf{a}_t | \phi(\mathbf{o}_{1:t}, \mathbf{a}_{1:t-1}))$ which aims at maximizing the expected return in a given RL problem. Here, we have a cyclic dependency, as the policy collects the trajectories to learn the representation by acting in the environment. In this setting, the policy's return and the sample complexity of the entire system determine what constitutes a *good* representation.

3.1 Representations from State Space Models

State Space Models (SSMs) [28] are commonly used to model time series data and naturally lend themselves to sensor fusion and information accumulation problems. We assume a latent state variable, \mathbf{z}_t , which evolves according to some Markovian dynamics $p(\mathbf{z}_{t+1}|\mathbf{z}_t, \mathbf{a}_t)$ given an action \mathbf{a}_t . At each time step t , each of the K observations is generated from the latent state by an observation model $p^{(k)}(\mathbf{o}_t^{(k)}|\mathbf{z}_t)$ and the initial state is distributed according to $p(\mathbf{z}_0)$. In this approach, the representation is given by (the parameters of) the belief over the latent state, taking into account all previous actions as well as previous and current observations $\phi(\mathbf{o}_{1:t}, \mathbf{a}_{1:t-1}) \triangleq p(\mathbf{z}_t|\mathbf{a}_{1:t-1}, \mathbf{o}_{1:t})$. Yet, due to the nonlinearity of the dynamics and observation models, computing $p(\mathbf{z}_t|\mathbf{a}_{1:t-1}, \mathbf{o}_{1:t})$ is intractable for models of relevant complexity. Thus, we approximate it using a variational distribution $q(\mathbf{z}_t|\mathbf{a}_{1:t-1}, \mathbf{o}_{1:t})$. This variational approximation plays an integral part in training the SSM and is thus readily available to use as input for the policy.

We instantiate the generative SSM and the variational distribution using a *Recurrent State Space Model (RSSM)* [14], which splits the latent state \mathbf{z}_t into a stochastic and a deterministic part. Following [14, 15], we assume the stochastic part of the *RSSM*'s latent state to be Gaussian, since the more recently introduced parametrization as a categorical distribution [16] has not been proven beneficial for the continuous control tasks considered in this work. While the original *RSSM* only has a single observation model $p(\mathbf{o}_t|\mathbf{z}_t)$, we extend it to K models, one for each observation modality. The variational distribution takes the deterministic part of the state together with the K observations $\mathbf{o}_t = \{\mathbf{o}_t^{(k)}\}_{k=1:K}$ and factorizes as $q(\mathbf{z}_{1:t}|\mathbf{o}_{1:t}, \mathbf{a}_{1:t-1}) = \prod_{t=1}^t q(\mathbf{z}_t|\mathbf{z}_{t-1}, \mathbf{a}_{t-1}, \mathbf{o}_t)$. Compared to the original *RSSM*, we again have to account for multiple observations instead of one. Thus, we first encode each observation individually using a set of K encoders, concatenate their outputs and provide the result to the *RSSM*. Finally, we also learn a reward model $p(r_t|\mathbf{z}_t)$ to predict the achieved reward from the representation. While predicting the reward from the latent state is conceptually only necessary for model-based RL, there is sufficient evidence in the literature that it is beneficial to also include it when learning representations for model-free RL [45, 49].

3.2 Learning the State Space Representation

We combine reconstruction-based and contrastive approaches to train our representations. Training *RSSMs* can be based on either a variational viewpoint [15, 25] or a contrastive predictive coding [33] viewpoint [30, 45]. We investigate both approaches, as neither decisively outperforms the other.

Variational Learning. Originally, [14] proposed leveraging a fully generative approach for *RSSMs*. Building on the stochastic variational autoencoding Bayes framework [22, 43], they derive a variational lower bound. After inserting our assumption that each observation factorizes into K independent observations and adding a term for reward prediction, this bound is given as

$$\sum_{t=1}^T \mathbb{E} \left[\sum_{k=1}^K \log p^{(k)}(\mathbf{o}_t^{(k)}|\mathbf{z}_t) + \log p(r_t|\mathbf{z}_t) - \text{KL}[q(\mathbf{z}_t|\mathbf{z}_{t-1}, \mathbf{a}_{t-1}, \mathbf{o}_t) \parallel p(\mathbf{z}_t|\mathbf{z}_{t-1}, \mathbf{a}_{t-1})] \right], \quad (1)$$

where the expectation is formed over the distribution $p(\mathbf{o}_{1:t}, \mathbf{a}_{1:t-1})q(\mathbf{z}_t|\mathbf{o}_{1:t}, \mathbf{a}_{1:t-1})$, i.e., sub-trajectories from a replay buffer and the variational distribution. Optimizing this bound using the reparametrization trick [22, 38] and stochastic gradient descent simultaneously trains the variational distribution and all parts of the generative model.

While this reconstruction-based approach can be highly effective, reconstructing high-dimensional, noisy observations can also cause issues. First, it requires introducing large parameter-rich observation models (usually up-convolutional neural nets for images) solely for representation learning. These observation models are unessential for the downstream task and are usually discarded after training. Second, the reconstruction forces the model to capture all details of the observations, which can lead to highly suboptimal representations if images are noisy or contain task-irrelevant distractions. Contrastive learning can provide a remedy to these problems. To introduce such contrastive terms, we can replace each individual log-likelihood term $\mathbb{E} \left[\log p^{(k)}(\mathbf{o}_t^{(k)}|\mathbf{z}_t) \right]$ with a corresponding mutual information (MI) term $I(\mathbf{o}_t^{(k)}, \mathbf{z}_t)$ by adding and subtracting the evidence $\log p(\mathbf{o}^{(k)})$ [15, 25]

$$\mathbb{E} \left[\log \left(p^{(k)}(\mathbf{o}_t^{(k)}|\mathbf{z}_t) / p(\mathbf{o}_t^{(k)}) \right) + \log p(\mathbf{o}_t^{(k)}) \right] = \mathbb{E} \left[I(\mathbf{o}_t^{(k)}, \mathbf{z}_t) \right] + c. \quad (2)$$

Intuitively, the MI measures how informative a given latent state is about the corresponding observations. Thus, maximizing it leads to similar latent states for similar sequences of observations and actions. While we cannot analytically compute the MI, we can estimate it using the InfoNCE bound [33, 35]. Doing so eliminates the need for generative reconstruction and instead only requires a discriminative approach based on a score function $f_v^{(k)}(\mathbf{o}_t^{(k)}, \mathbf{z}_t) \mapsto \mathbb{R}_+$. This score function measures the compatibility of pairs of observations and latent states. It shares large parts of its parameters with the *RSSM*. For details on the exact parameterization, we refer to [Appendix B](#).

Crucially, this methodology allows the mixing of reconstruction and mutual information terms for the individual sensors, resulting in

$$\sum_{t=1}^T \sum_{k=1}^K \mathcal{L}_v^{(k)}(\mathbf{o}_t^{(k)}, \mathbf{z}_t) + \mathbb{E}[\log p(r_t | \mathbf{z}_t) - \text{KL}[q(\mathbf{z}_t | \mathbf{z}_{t-1}, \mathbf{a}_{t-1}, \mathbf{o}_t) \parallel p(\mathbf{z}_t | \mathbf{z}_{t-1}, \mathbf{a}_{t-1})]], \quad (3)$$

where $\mathcal{L}_v^{(k)}$ is either the log-likelihood or the MI term. As we show in [Section 4](#) choosing the terms corresponding to the properties of the corresponding modality can often improve performance.

Contrastive Predictive Coding. CPC [33] provides an alternative to the variational approach. The idea is to maximize the MI between the latent variable \mathbf{z}_t and the next observation $\mathbf{o}_{t+1}^{(k)}$, i. e., $I(\mathbf{o}_{t+1}^{(k)}, \mathbf{z}_t)$. While this approach seems similar to contrastive variational learning, there is a crucial conceptual difference. We estimate the MI between the current latent state and the next observation, not the current observation. Thus, we explicitly predict one step ahead to compute the loss. As we use the *RSSM*'s dynamics model for the prediction, this formalism provides a training signal to the dynamics model. However, prior works [42, 30, 45] showed that solely optimizing for prediction is insufficient. We follow [45] and regularize the objective further by a reward prediction term, the KL-term from [Equation 1](#) multiplied with a small factor β , and an inverse dynamics predictor $\hat{\mathbf{a}}_t = a(\mathbf{z}_t, \mathbf{z}_{t+1})$. Here, $\hat{\mathbf{a}}_t$ is trained to predict the action from two consecutive latent states by minimizing $l_a = \|\mathbf{a}_t - \hat{\mathbf{a}}_t\|^2$. Additionally, we can turn individual contrastive MI terms into explicit reconstruction terms for suitable sensor modalities by reversing the principle introduced in [Equation 2](#). This approach results in the following maximization objective

$$\sum_{t=1}^T \sum_{k=1}^K \mathcal{L}_p^{(k)}(\mathbf{o}_{t+1}^{(k)}, \mathbf{z}_t) + \mathbb{E}[\log p(r_t | \mathbf{z}_t) - \beta \text{KL}[q(\mathbf{z}_t | \mathbf{z}_{t-1}, \mathbf{a}_{t-1}, \mathbf{o}_t) \parallel p(\mathbf{z}_t | \mathbf{z}_{t-1}, \mathbf{a}_{t-1})] - l_a], \quad (4)$$

where $\mathcal{L}_p^{(k)}$ is either the one-step ahead likelihood $\log p(\mathbf{o}_{t+1}^{(k)} | \mathbf{z}_t)$ or an InfoNCE estimate of $I(\mathbf{o}_{t+1}^{(k)}, \mathbf{z}_t)$ using a score function $f_p^{(k)}(\mathbf{o}_{t+1}^{(k)}, \mathbf{z}_t) \mapsto \mathbb{R}_+$. From an implementation viewpoint, the resulting approach differs only slightly from the variational contrastive one. For CPC approaches, we use a sample from the *RSSM*'s dynamics $p(\mathbf{z}_{t+1} | \mathbf{z}_t, \mathbf{a}_t)$ and for contrastive variational approaches we use a sample from the variational distribution $q(\mathbf{z}_t | \mathbf{z}_{t-1}, \mathbf{a}_{t-1}, \mathbf{o}_t)$.

Estimating Mutual Information with InfoNCE. We estimate the mutual information (MI) using b mini-batches of sub-sequences of length l . After computing the latent estimates, we get $I = b \cdot l$ pairs $(\mathbf{o}_i, \mathbf{z}_i)$, i. e., we use both samples from the elements of the batch as well as all the other time steps within the sequence as negative samples. Using those, the symmetry of MI, the InfoNCE bound [35], and either $f = f_v^{(k)}$ or $f = f_p^{(k)}$, we can estimate the MI as

$$0.5 \left(\sum_{i=1}^I \log \frac{f(\mathbf{z}_i, \mathbf{o}_i)}{\sum_{j=1}^I f(\mathbf{z}_j, \mathbf{o}_i)} + \log \frac{f(\mathbf{z}_i, \mathbf{o}_i)}{\sum_{j=1}^I f(\mathbf{z}_i, \mathbf{o}_j)} \right).$$

Image Augmentation. Following prior works [45, 7], we found image augmentation helpful for contrastive approaches. During training, crops are randomly selected for each sequence but remain consistent within the sequence. For evaluation, we crop at the center.

3.3 Learning to Act Based on the Representation

Given the learned representation, we consider both model-based and model-free reinforcement learning. For model-free RL, we use Soft Actor-Critic (SAC) [13] on top of the representation. More specifically, we use the deterministic part of the latent state and the mean of the stochastic part as

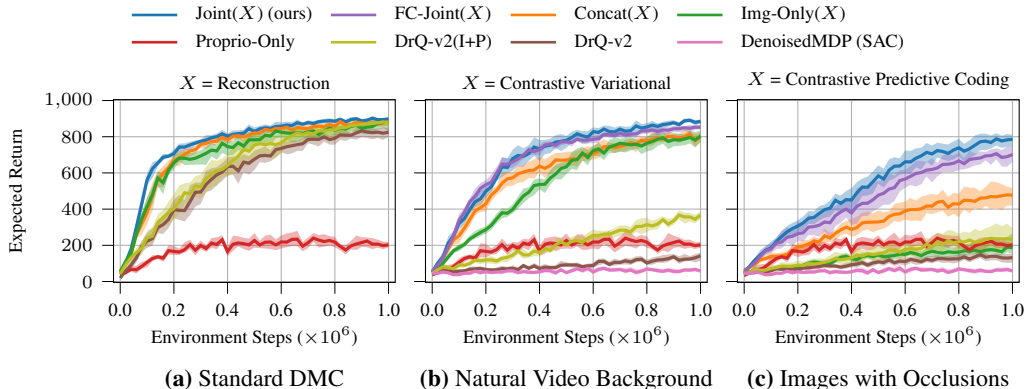


Figure 2: Excerpt of the aggregated results for **model-free** agents on the DMC Suite tasks with different forms of image observations. In all tasks using proprioception is beneficial. More importantly, learning a joint representation outperforms the concatenation of image representations and proprioception. **(a)**: Reconstruction on the standard images. Even though the images provide all information necessary to solve the tasks, our method can still exploit the proprioceptive information and improve upon the image-only baselines and *DRQ-v2(I+P)* in both sample efficiency and final performance. **(b)**: Contrastive variational approaches on natural video background tasks. While the concatenation initially learns faster than image-only representations, only joint representations substantially improve the final performance. **(c)**: Contrastive predictive coding approaches on occlusion tasks. No approach using a single sensor is capable of solving this task. However, using both images and proprioception can give good results, in particular when combining a contrastive loss for the images with reconstruction for the proprioception.

input to both the actor and the critic. In the model-based setting, we use latent imagination [15], which propagates gradients directly through the learned dynamics model to optimize the actor. In the case of pure reconstruction-based representation, this approach defaults to the original *Dreamer* [15]. In both cases, we alternately update the *RSSM*, actor, and critic for several steps before collecting a new sequence in the environment. Furthermore, the *RSSM* uses only the representation learning loss and gets neither gradients from the actor nor the critic.

4 Experiments

We evaluate our joint representation learning approach on several environments from the DeepMind Control (DMC) Suite [47] with different types of image observations and a new *Locomotion Suite*. We train five seeds per task for 10^6 environment steps and evaluate for 20 rollouts every 20,000 steps. Following the suggestions from [1], we aggregate the results over all environments in the benchmark suites and report interquartile means and 95% stratified bootstrapped confidence intervals, indicated by shaded areas. For experimental details, we refer to [Appendix B](#). In summary, we compare the following approaches.

Joint Representation Learning. We denote all our joint representations approaches with *Joint(X)*. Here, X will denote how we trained the representation, which is either pure reconstruction (R) (Equation 1), or a mixture of a contrastive image loss and reconstruction for the proprioception. The former is either the contrastive variational objective (CV , i.e., Equation 3) or the contrastive predictive objective (CPC , i.e., Equation 4). For both contrastive methods, we also evaluate using the contrastive loss for both image and proprioception. We denote these fully contrastive approaches by *FC-Joint(CV)* and *FC-Joint(CPC)*.

Concatenating Representations. One important baseline is concatenating the proprioception to a representation trained solely on images. To ensure a fair comparison, we train this representation using our approach only on images. Here, we again use reconstruction and both contrastive methods for training and refer to the resulting approaches as *Concat(R)*, *Concat(CV)*, and *Concat(CPC)*. We consider this baseline only for the model-free setting as it cannot predict future proprioception which renders model-based RL infeasible.

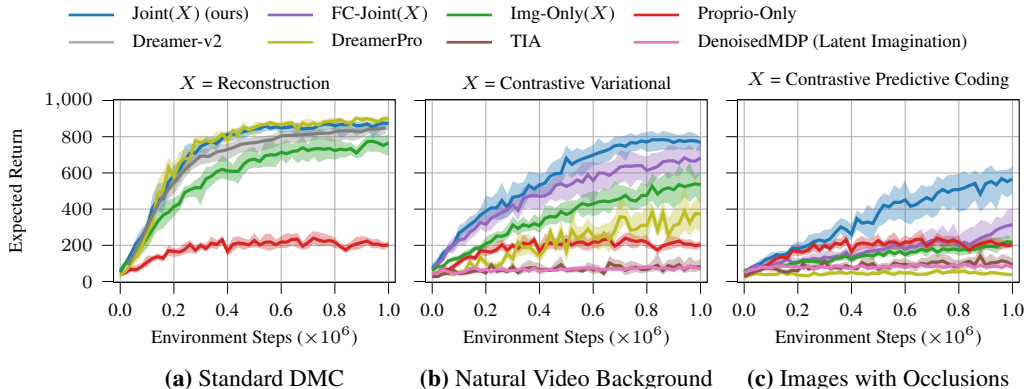


Figure 3: Excerpt of the aggregated results for **model-based** agents on the DMC Suite tasks, with different forms of image observations. **(a)**: Reconstruction on the standard images. $Img\text{-}Only(R)$, which almost corresponds to the original Dreamer[15], performs slightly worse than $Dreamer\text{-}v2$ and $DreamerPro$, while this performance gap is closed by $Joint(X)$. **(b)**: Contrastive variational approaches on natural video background tasks. Compared with the standard image tasks, both $DreamerPro$ s’ and $Img\text{-}Only(CV)$ s’ performance decreases significantly, while the joint representation learning with a mixture of contrastive and reconstruction ($Joint(CV)$) almost achieves the same final performance as reconstruction without distractions. **(c)**: Contrastive predictive coding approaches on occlusion tasks. Only the combined joint objective performs significantly better than the proprioception-only baseline.

Single Observations. We also train policies using only a single sensor to ensure our approaches can exploit the additional information provided by multiple sensors. For the image-only policies, we again use our state space representation learning approach with the different training schemes, resulting in $Img\text{-}Only(R)$, $Img\text{-}Only(CV)$, and $Img\text{-}Only(CPC)$. For the proprioception-only policies ($Proprio\text{-}Only$), we use SAC [13] directly on the proprioception without learning an explicit representation.

Related Approaches. We compare to several model-based $RSSM$ approaches. We consider the reconstruction $Dreamer\text{-}v2$ [16] and the contrastive $DreamerPro$ [7], which builds on prototypical representations. Additionally, we compare against TIA [10] and the $DenoisedMDP$ [51]. Both propose special losses and factorizations of the latent space to allow disentangling task-relevant from irrelevant aspects. $DenoisedMDP$ also provides both, model-based and model-free versions, and we compare with both. Furthermore, we compare to the model-free $DrQ\text{-}v2$ [57], as well as an extension that uses images and proprioception ($DrQ\text{-}v2(I+P)$). Both do not explicitly learn a representation. Finally, $Img\text{-}Only(R)$ with model-based RL corresponds mostly to Dreamer-v1 [15] and $Img\text{-}Only(CPC)$ as well as $FC\text{-}Joint(CPC)$ with model-free RL closely resemble the approach introduced in [45]. Appendix A.3 provides details on the differences.

4.1 DeepMind Control Suite

We use seven tasks from the DMC Suite [47], namely Ball-in-Cup Catch, Cartpole Swingup, Cheetah Run, Reacher Easy, Walker Walk, Walker Run, and Quadruped Walk. For each task, we split the state into proprioceptive entries and non-proprioceptive entries. While the former is directly provided, the latter can only be perceived via an additional image. For example, in Ball in Cup Catch the cup’s state is proprioceptive while the ball’s state needs to be inferred from the image. Appendix A lists the details for all considered environments. Besides standard images, we run experiments with two types of modified images by adding natural video backgrounds or occlusions. The latter renders the tasks much more challenging due to the additional partial observability. The upper row of Figure 4 shows examples of these image modifications.

Natural Video Background. Following [30, 7] we render random videos from the Kinetics400 dataset [20] behind the agent. The challenge of this task is to learn a representation that filters out as many irrelevant visual details as possible while not ignoring relevant aspects. Methods based on image reconstruction struggle at this task as they are forced to model all background details to minimize their objective. While contrastive approaches can ignore parts of the image, the challenge is to formulate an objective that focuses exclusively on the relevant details.

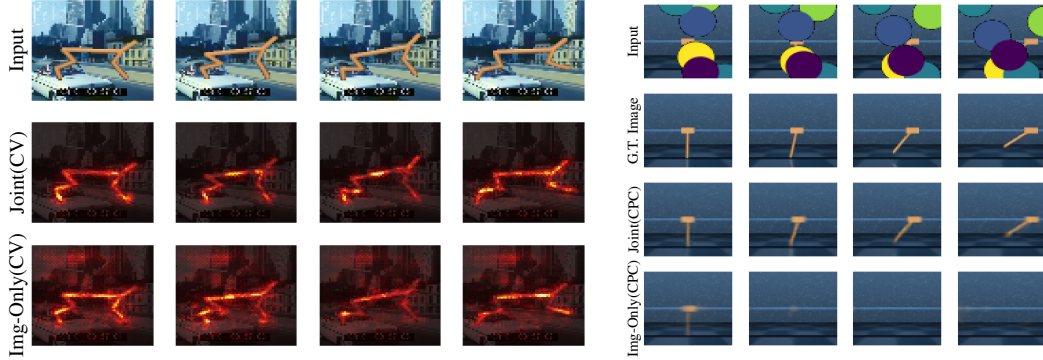


Figure 4: **Left:** Saliency Maps (pixel-wise norm of the Jacobian of the latent representation w.r.t. the image) showing on which pixels the respective representation learning approaches focus. *Joint(CV)* clearly focuses better on the task-relevant cheetah, while the *Img-Only(CV)* is more distracted by the background video. **Right:** We provide occluded images and train an additional decoder to reconstruct the occlusion-free ground truth from the (detached) latent representation. For *Cartpole Swingup* only the cart position is part of the proprioception, while the pole angle has to be inferred from the images. Still, the *Joint(CPC)* is able to capture both cart position and pole angle, while *Img-Only(CPC)* clearly fails to do so. Both examples illustrate how using proprioception in representation can guide representation learning to focus on and capture the relevant parts of the image.

Images with Occlusions. We render occlusions by adding disks that slowly move in front of the agent. Those occlusions can hide relevant information in the images for multiple consecutive time steps, which decreases observability and increases the task’s complexity. This modification tests the capabilities of the approaches not to be distracted by the easily predictable disks, and to maintain a consistent representation across multiple time steps when relevant aspects are missing for some images.

Results. Figure 2 shows an excerpt of the results for model-free agents. Joint representations generally outperform the concatenation and single-sensor approaches. They perform best when trained with our combination of reconstruction-based and contrastive losses and outperform all model-free and model-based baselines in the natural video background and occlusion tasks. In particular, learning joint representations performs better than providing the same information by concatenating an image representation and the proprioception. As expected, none of the pure reconstruction approaches can solve the natural video and occlusion tasks, while methods that use a contrastive loss for the images are less affected by the distractors or occlusions. For the occluded tasks, all image-only approaches struggle to learn any reasonable behavior, underscoring the difficulty of the task. Figure 3 shows an excerpt of the results for model-based agents. Again, the benefits of joint representation learning with a combined objective become clear. While the performance of the contrastive image-only approaches decreases when adding natural video backgrounds, *Joint(CV)* still achieves high performance. This result demonstrates how joint representations allow learning of stable long-term dynamics that enable successful model-based RL. In the occlusion setting, the contrastive predictive approach also performs best, while the image-only approaches cannot compete with the proprioception-only baseline. However, for contrastive image losses, all model-based approaches perform worse than their model-free counterparts, indicating that the dynamics can still be improved. *TIA* and *DenoisedMDP* fail in both our natural video and occlusion tasks because they explicitly model the natural videos and occlusions. The discrepancy in performance reported in the original works for these approaches on natural videos is due to changes in the experimental setup. We refer to Appendix A.3 for details. Appendix C provides the full experimental results of all methods on all image types and for the individual environments. Finally, we further investigate some of the learned representations in Figure 4, which illustrates how joint representation learning can guide the approaches to focus on relevant aspects of an environment while not being distracted by irrelevant noise.

4.2 Locomotion Suite

We propose a novel benchmark consisting of six locomotion tasks. For all tasks, we use proprioception and egocentric images. The agents need the proprioception to be aware of their own state, as they

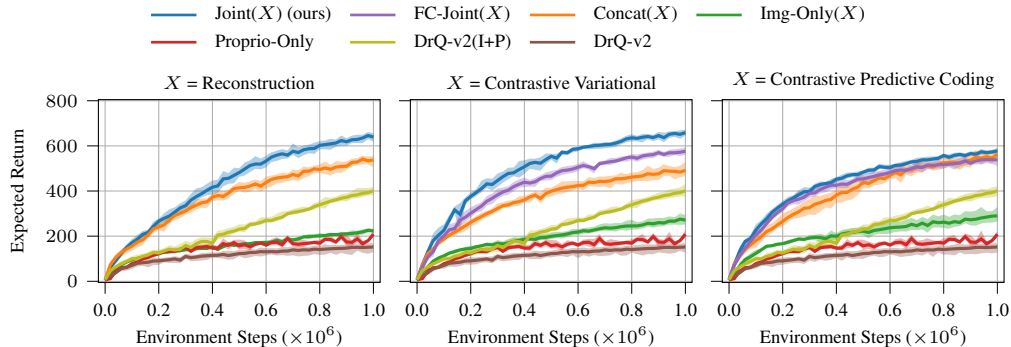


Figure 5: Aggregated results for all environments of the locomotion suite. Learning joint representations gives the best results with all approaches for representation learning. The joint representations clearly outperform concatenating image representations and proprioception, as well as *DRQ-v2* and *DRQ-v2 (I+P)*. Combining a contrastive loss for the image with reconstruction for the proprioception is better than solely relying on contrastive losses. On these tasks, the contrastive variational approach again outperforms contrastive predictive coding and, in terms of sample efficiency, even the reconstruction.

cannot observe themselves from the egocentric perspective. Moreover, the agents require egocentric images to avoid obstacles whose position and size are only available through the image. Three tasks are readily available with the DeepMind Control Suite [47] and the software stack introduced in [48]. We designed three more by introducing hurdles into the Cheetah Run, Walker Walk, and Walker Run tasks. In these new environments, agents need to identify the location and size of "hurdles" placed in their way in order to jump over them while moving forward. Figure 1 shows examples for the modified Cheetah Run. Appendix A.2 provides details about all environments. We focus our evaluation on model-free approaches, as those outperformed the model-based ones in the previous experiment. The results in Figure 5 support the previous findings that using joint representations improves over concatenating image representations with proprioception. Again, approaches that combine contrastive and reconstruction losses outperform those using only contrastive losses. These results further demonstrate the benefits of learning joint representations, even in tasks where distractions play no role.

5 Conclusion

We consider the problem of Reinforcement Learning (RL) from multiple sensors, in particular images and proprioception. Building on *Recurrent State Space Models* [14], we learn joint representations of all available sensors instead of considering them in isolation. We propose combining contrastive and reconstruction approaches considering variational and predictive coding paradigms for training. In our large-scale evaluation, we show the benefits of this approach for both model-free and model-based RL. For model-free RL, joint representations outperform the concatenation of image representations and proprioception. Using the proprioception in representation learning can guide the approach to focus on and capture all relevant aspects of the images, allowing to solve tasks where current image-only approaches fail. For model-based agents, our joint representations offer an easy and highly effective alternative to improve performance for tasks that require contrastive image objectives.

Limitations. While we showed the benefits of joint representations in both cases, our evaluation is inconclusive about whether the variational or predictive coding approach is preferable. Additionally, even with a combination of contrastive and reconstruction losses, model-free agents perform better than their model-based counterparts. As both types of agents perform equally well for pure reconstruction, this suggests there is still room for improvement in contrastive *RSSM* training, especially w.r.t. learning the dynamics. Furthermore, our current approach assumes all modalities are available for all sequences and cannot exploit large amounts of data available for individual sensors, e.g., images. Studying how to include such data or existing image representations [34, 54, 29, 26] into our joint representation learning framework is a promising avenue for future research.

Broader Impact. While we do not foresee any immediate negative societal impacts of our work, improved representations for RL might ultimately lead to more capable autonomous systems, which can have both positive and negative effects. We believe identifying and mitigating the potentially harmful effects of such autonomous systems is the responsibility of sovereign governments.

References

- [1] Rishabh Agarwal, Max Schwarzer, Pablo Samuel Castro, Aaron C Courville, and Marc Bellemare. Deep reinforcement learning at the edge of the statistical precipice. *Advances in neural information processing systems*, 34:29304–29320, 2021.
- [2] Jimmy Lei Ba, Jamie Ryan Kiros, and Geoffrey E Hinton. Layer normalization. *arXiv preprint arXiv:1607.06450*, 2016.
- [3] Ershad Banijamali, Rui Shu, Hung Bui, Ali Ghodsi, et al. Robust locally-linear controllable embedding. In *International Conference on Artificial Intelligence and Statistics*, pages 1751–1759. PMLR, 2018.
- [4] Philipp Becker and Gerhard Neumann. On uncertainty in deep state space models for model-based reinforcement learning. *Transactions on Machine Learning Research*, 2022.
- [5] Anthony Brohan, Yevgen Chebotar, Chelsea Finn, Karol Hausman, Alexander Herzog, Daniel Ho, Julian Ibarz, Alex Irpan, Eric Jang, Ryan Julian, et al. Do as i can, not as i say: Grounding language in robotic affordances. In *6th Annual Conference on Robot Learning*, 2022.
- [6] Kyunghyun Cho, Bart Van Merriënboer, Dzmitry Bahdanau, and Yoshua Bengio. On the properties of neural machine translation: Encoder-decoder approaches. *arXiv preprint arXiv:1409.1259*, 2014.
- [7] Fei Deng, Ingoon Jang, and Sungjin Ahn. Dreamerpro: Reconstruction-free model-based reinforcement learning with prototypical representations. In *International Conference on Machine Learning*, pages 4956–4975. PMLR, 2022.
- [8] Danny Driess, Fei Xia, Mehdi SM Sajjadi, Corey Lynch, Aakanksha Chowdhery, Brian Ichter, Ayzaan Wahid, Jonathan Tompson, Quan Vuong, Tianhe Yu, et al. Palm-e: An embodied multimodal language model. *arXiv preprint arXiv:2303.03378*, 2023.
- [9] Chelsea Finn, Ian Goodfellow, and Sergey Levine. Unsupervised learning for physical interaction through video prediction. *Advances in neural information processing systems*, 29, 2016.
- [10] Xiang Fu, Ge Yang, Pulkit Agrawal, and Tommi Jaakkola. Learning task informed abstractions. In *International Conference on Machine Learning*, pages 3480–3491. PMLR, 2021.
- [11] Zipeng Fu, Ashish Kumar, Ananye Agarwal, Haozhi Qi, Jitendra Malik, and Deepak Pathak. Coupling vision and proprioception for navigation of legged robots. In *Proceedings of the IEEE/CVF Conference on Computer Vision and Pattern Recognition (CVPR)*, pages 17273–17283, June 2022.
- [12] David Ha and Jürgen Schmidhuber. World models. *arXiv preprint arXiv:1803.10122*, 2018.
- [13] Tuomas Haarnoja, Aurick Zhou, Kristian Hartikainen, George Tucker, Sehoon Ha, Jie Tan, Vikash Kumar, Henry Zhu, Abhishek Gupta, Pieter Abbeel, et al. Soft actor-critic algorithms and applications. *arXiv preprint arXiv:1812.05905*, 2018.
- [14] Danijar Hafner, Timothy Lillicrap, Ian Fischer, Ruben Villegas, David Ha, Honglak Lee, and James Davidson. Learning latent dynamics for planning from pixels. In *International conference on machine learning*, pages 2555–2565. PMLR, 2019.
- [15] Danijar Hafner, Timothy Lillicrap, Jimmy Ba, and Mohammad Norouzi. Dream to control: Learning behaviors by latent imagination. In *International Conference on Learning Representations*, 2020.

- [16] Danijar Hafner, Timothy P Lillicrap, Mohammad Norouzi, and Jimmy Ba. Mastering atari with discrete world models. In *International Conference on Learning Representations*, 2021.
- [17] Danijar Hafner, Kuang-Huei Lee, Ian Fischer, and Pieter Abbeel. Deep hierarchical planning from pixels. In *Advances in Neural Information Processing Systems*, 2022.
- [18] Danijar Hafner, Jurgis Pasukonis, Jimmy Ba, and Timothy Lillicrap. Mastering diverse domains through world models. *arXiv preprint arXiv:2301.04104*, 2023.
- [19] Dmitry Kalashnikov, Alex Irpan, Peter Pastor, Julian Ibarz, Alexander Herzog, Eric Jang, Deirdre Quillen, Ethan Holly, Mrinal Kalakrishnan, Vincent Vanhoucke, et al. Scalable deep reinforcement learning for vision-based robotic manipulation. In *Conference on Robot Learning*, pages 651–673. PMLR, 2018.
- [20] Will Kay, Joao Carreira, Karen Simonyan, Brian Zhang, Chloe Hillier, Sudheendra Vijayanarasimhan, Fabio Viola, Tim Green, Trevor Back, Paul Natsev, et al. The kinetics human action video dataset. *arXiv preprint arXiv:1705.06950*, 2017.
- [21] Diederik P Kingma and Jimmy Ba. Adam: A method for stochastic optimization. In *ICLR*, 2015.
- [22] Diederik P Kingma and Max Welling. Auto-encoding variational bayes. *arXiv preprint arXiv:1312.6114*, 2013.
- [23] Alex X Lee, Anusha Nagabandi, Pieter Abbeel, and Sergey Levine. Stochastic latent actor-critic: Deep reinforcement learning with a latent variable model. *Advances in Neural Information Processing Systems*, 33:741–752, 2020.
- [24] Sergey Levine, Chelsea Finn, Trevor Darrell, and Pieter Abbeel. End-to-end training of deep visuomotor policies. *The Journal of Machine Learning Research*, 17(1):1334–1373, 2016.
- [25] Xiao Ma, Siwei Chen, David Hsu, and Wee Sun Lee. Contrastive variational reinforcement learning for complex observations. In *Conference on Robot Learning*, pages 959–972. PMLR, 2020.
- [26] Arjun Majumdar, Karmesh Yadav, Sergio Arnaud, Yecheng Jason Ma, Claire Chen, Sneha Silwal, Aryan Jain, Vincent-Pierre Berges, Pieter Abbeel, Jitendra Malik, et al. Where are we in the search for an artificial visual cortex for embodied intelligence? *arXiv preprint arXiv:2303.18240*, 2023.
- [27] Oier Mees, Lukas Hermann, and Wolfram Burgard. What matters in language conditioned robotic imitation learning over unstructured data. *IEEE Robotics and Automation Letters*, 7(4): 11205–11212, 2022.
- [28] Kevin P Murphy. *Machine learning: a probabilistic perspective*. MIT press, 2012.
- [29] Suraj Nair, Aravind Rajeswaran, Vikash Kumar, Chelsea Finn, and Abhinav Gupta. R3m: A universal visual representation for robot manipulation. In *6th Annual Conference on Robot Learning*, 2022.
- [30] Tung D Nguyen, Rui Shu, Tuan Pham, Hung Bui, and Stefano Ermon. Temporal predictive coding for model-based planning in latent space. In *International Conference on Machine Learning*, pages 8130–8139. PMLR, 2021.
- [31] Masashi Okada and Tadahiro Taniguchi. Dreaming: Model-based reinforcement learning by latent imagination without reconstruction. In *2021 IEEE International Conference on Robotics and Automation (ICRA)*, pages 4209–4215. IEEE, 2021.
- [32] Masashi Okada and Tadahiro Taniguchi. Dreamingv2: Reinforcement learning with discrete world models without reconstruction. In *2022 IEEE/RSJ International Conference on Intelligent Robots and Systems (IROS)*, pages 985–991. IEEE, 2022.
- [33] Aaron van den Oord, Yazhe Li, and Oriol Vinyals. Representation learning with contrastive predictive coding. *arXiv preprint arXiv:1807.03748*, 2018.

- [34] Simone Parisi, Aravind Rajeswaran, Senthil Purushwalkam, and Abhinav Gupta. The unsurprising effectiveness of pre-trained vision models for control. In *International Conference on Machine Learning*, pages 17359–17371. PMLR, 2022.
- [35] Ben Poole, Sherjil Ozair, Aaron Van Den Oord, Alex Alemi, and George Tucker. On variational bounds of mutual information. In *International Conference on Machine Learning*, pages 5171–5180. PMLR, 2019.
- [36] Alec Radford, Jong Wook Kim, Chris Hallacy, Aditya Ramesh, Gabriel Goh, Sandhini Agarwal, Girish Sastry, Amanda Askell, Pamela Mishkin, Jack Clark, et al. Learning transferable visual models from natural language supervision. In *International Conference on Machine Learning*, pages 8748–8763. PMLR, 2021.
- [37] Aditya Ramesh, Prafulla Dhariwal, Alex Nichol, Casey Chu, and Mark Chen. Hierarchical text-conditional image generation with clip latents. *arXiv preprint arXiv:2204.06125*, 2022.
- [38] Danilo Jimenez Rezende, Shakir Mohamed, and Daan Wierstra. Stochastic backpropagation and approximate inference in deep generative models. In *International conference on machine learning*, pages 1278–1286. PMLR, 2014.
- [39] Younggyo Seo, Danijar Hafner, Hao Liu, Fangchen Liu, Stephen James, Kimin Lee, and Pieter Abbeel. Masked world models for visual control. In *6th Annual Conference on Robot Learning*, 2022.
- [40] Mohit Shridhar, Lucas Manuelli, and Dieter Fox. Cliport: What and where pathways for robotic manipulation. In *Conference on Robot Learning*, pages 894–906. PMLR, 2022.
- [41] Mohit Shridhar, Lucas Manuelli, and Dieter Fox. Perceiver-actor: A multi-task transformer for robotic manipulation. In *Conference on Robot Learning*, pages 785–799. PMLR, 2023.
- [42] Rui Shu, Tung Nguyen, Yinlam Chow, Tuan Pham, Khoat Than, Mohammad Ghavamzadeh, Stefano Ermon, and Hung Bui. Predictive coding for locally-linear control. In *International Conference on Machine Learning*, pages 8862–8871. PMLR, 2020.
- [43] Kihyuk Sohn, Honglak Lee, and Xinchun Yan. Learning structured output representation using deep conditional generative models. *Advances in neural information processing systems*, 28: 3483–3491, 2015.
- [44] Aravind Srinivas, Michael Laskin, and Pieter Abbeel. Curl: Contrastive unsupervised representations for reinforcement learning. *arXiv preprint arXiv:2004.04136*, 2020.
- [45] Nitish Srivastava, Walter Talbott, Martin Bertran Lopez, Shuangfei Zhai, and Joshua M. Susskind. Robust robotic control from pixels using contrastive recurrent state-space models. In *Deep RL Workshop NeurIPS 2021*, 2021.
- [46] Adam Stooke, Kimin Lee, Pieter Abbeel, and Michael Laskin. Decoupling representation learning from reinforcement learning. In *International Conference on Machine Learning*, pages 9870–9879. PMLR, 2021.
- [47] Yuval Tassa, Yotam Doron, Alistair Muldal, Tom Erez, Yazhe Li, Diego de Las Casas, David Budden, Abbas Abdolmaleki, Josh Merel, Andrew Lefrancq, et al. Deepmind control suite. *arXiv preprint arXiv:1801.00690*, 2018.
- [48] Yuval Tassa, Saran Tunyasuvunakool, Alistair Muldal, Yotam Doron, Siqi Liu, Steven Bohez, Josh Merel, Tom Erez, Timothy Lillicrap, and Nicolas Heess. dm_control: Software and tasks for continuous control. *Software Impacts*, 6:100022, 2020.
- [49] Manan Tomar, Utkarsh Aashu Mishra, Amy Zhang, and Matthew E Taylor. Learning representations for pixel-based control: What matters and why? *Transactions on Machine Learning Research*, 2023.
- [50] Niklas Wahlström, Thomas B Schön, and Marc Peter Deisenroth. From pixels to torques: Policy learning with deep dynamical models. *arXiv preprint arXiv:1502.02251*, 2015.

- [51] Tongzhou Wang, Simon Du, Antonio Torralba, Phillip Isola, Amy Zhang, and Yuandong Tian. Denoised mdps: Learning world models better than the world itself. In *International Conference on Machine Learning*, pages 22591–22612. PMLR, 2022.
- [52] Manuel Watter, Jost Springenberg, Joschka Boedecker, and Martin Riedmiller. Embed to control: A locally linear latent dynamics model for control from raw images. In *Advances in neural information processing systems*, pages 2746–2754, 2015.
- [53] Philipp Wu, Alejandro Escontrela, Danijar Hafner, Pieter Abbeel, and Ken Goldberg. Daydreamer: World models for physical robot learning. In *6th Annual Conference on Robot Learning*, 2022.
- [54] Tete Xiao, Ilija Radosavovic, Trevor Darrell, and Jitendra Malik. Masked visual pre-training for motor control. *arXiv preprint arXiv:2203.06173*, 2022.
- [55] Denis Yarats, Rob Fergus, Alessandro Lazaric, and Lerrel Pinto. Reinforcement learning with prototypical representations. In *International Conference on Machine Learning*, pages 11920–11931. PMLR, 2021.
- [56] Denis Yarats, Amy Zhang, Ilya Kostrikov, Brandon Amos, Joelle Pineau, and Rob Fergus. Improving sample efficiency in model-free reinforcement learning from images. In *Proceedings of the AAAI Conference on Artificial Intelligence*, volume 35, pages 10674–10681, 2021.
- [57] Denis Yarats, Rob Fergus, Alessandro Lazaric, and Lerrel Pinto. Mastering visual continuous control: Improved data-augmented reinforcement learning. In *International Conference on Learning Representations*, 2022.
- [58] Bang You, Oleg Arenz, Youping Chen, and Jan Peters. Integrating contrastive learning with dynamic models for reinforcement learning from images. *Neurocomputing*, 476:102–114, 2022.
- [59] Amy Zhang, Rowan Thomas McAllister, Roberto Calandra, Yarín Gal, and Sergey Levine. Learning invariant representations for reinforcement learning without reconstruction. In *International Conference on Learning Representations*, 2020.

Table 1: Splits of the entire system state into proprioceptive and non-proprioceptive parts for the DeepMind Control Suite environments.

Environment	Proprioceptive	Non-Proprioceptive
Ball In Cup	cup position and velocity	ball position and velocity
Cartpole	cart position and velocity	pole angle and velocity
Cheetah	joint positions and velocities	global pose and velocity
Reacher	reacher position and velocity	distance to target
Quadruped	joint positions and velocities	global pose + velocity, forces
Walker	orientations and velocities of links	global pose and velocity, height above ground

Table 2: Splits of the entire system state into proprioceptive and non-proprioceptive parts for the Locomotion Suite. Some of the agents (Cheetah, Walker, Quadruped) require more proprioceptive information for the locomotion tasks with an egocentric vision than for the standard tasks with images from an external perspective.

Environment	Proprioceptive	Non-Proprioceptive
Ant	joint position and velocity global velocities	wall positions global position
Hurdle Cheetah	joint positions and velocities global velocity	hurdle positions and heights global position
Hurdle Walker	orientations and velocities of links	hurdle positions and height global position and velocity
Quadruped (Escape)	joint positions and velocities, torso orientation and velocity, imu, forces, and torques at joints	Information about terrain

A Environments and Baselines

A.1 DeepMind Control Suite Tasks

Table 1 states how we split the states of the original DeepMind Control Suite [47] tasks into proprioceptive and non-proprioceptive parts. For the model-based agents, we followed common practice [15, 10, 51, 7] and use an action repeat of 2 for all environments. We do the same for the model-free agents except for: Ball In Cup Catch (4), Cartpole Swingup (8), Cheetah Run (4) and Reacher Easy (4). All environments in the locomotion suite also use an action repeat of 2, this includes Hurdle Cheetah Run which requires more fine-grained control than the normal version to avoid the hurdles.

Natural Background. Following [30, 7, 59, 10, 51] we render videos from the `driving_car` class of the Kinetics400 dataset [20] behind the agents to add a natural video background. However, the previously mentioned works implement this idea in two distinct ways. [30] and [7] use color images as background and pick a random sub-sequence of a random video for each environment rollout. They adhere to the train-validation split of the Kinetics400 dataset, using training videos for representation and policy learning and validation videos during evaluation. [59, 10, 51], according to the official implementations, instead work with gray-scale images and sample a single background video for the train set once during initialization of the environment. They do not sample a new video during the environment reset, thus all training sequences have the same background video. We follow the first approach, as we believe it mimics a more realistic scenario of always changing and colored natural background.

Occlusions. Following [4], we rendered slow-moving disks over the original observations to occlude parts of the observation. The speed of the disks makes memory necessary, as they can occlude relevant aspects for multiple consecutive timesteps.

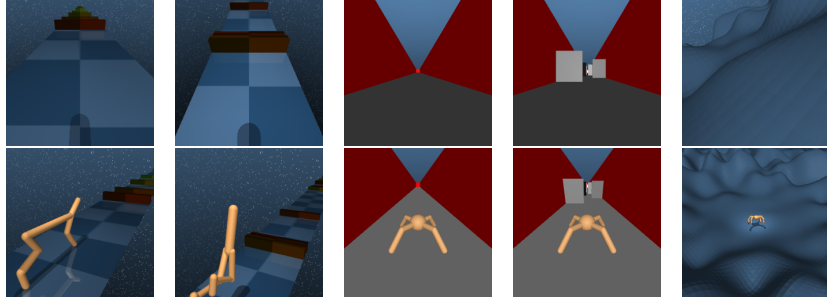


Figure 6: The environments in the Locomotion Suite are (from left to right) Hurdle Cheetah Run, Hurdle Walker Walk / Run, Ant Empty, Ant Walls, and Quadruped Escape. **Upper Row:** Egocentric vision provided to the agent. **Lower Row:** External image for visualization.

A.2 Locomotion Suite

The 6 tasks in the locomotion suite are Ant Empty, Ant Walls, Hurdle Cheetah Run, Hurdle Walker Walk, Hurdle Walker Run, and Quadruped Escape. Table 2 shows the splits into proprioceptive and non-proprioceptive parts. Figure 6 displays all environments in the suite.

Ant. The Ant tasks build on the locomotion functionality introduced into the DeepMind Control suite by [48]. For Ant Empty, we only use an empty corridor, which makes this the easiest task in our locomotion suite. For Ant Walls, we randomly generate walls inside the corridor, and the agent has to avoid those in order to achieve its goal, i.e., running through the corridor as fast as possible.

Hurdle Cheetah & Walker. We modified the standard Cheetah Run, Walker Walk, and Walker Run tasks by introducing "hurdles" over which the agent has to step in order to move forward. The hurdles' positions, heights, and colors are reset randomly for each episode, and the agent has to perceive them using egocentric vision. For this vision, we added a camera in the head of the Cheetah and Walker.

Quadruped Escape. The Quadruped Escape task is readily available in the DeepMind Control Suite. For the egocentric vision, we removed the range-finding sensors from the original observation and added an egocentric camera.

A.3 Baselines.

For *Dreamer-V2*[16] we use the raw reward curve data provided with the official implementation². For *DreamerPro*[7]³, *TIA*[10]⁴, *DenoisedMDP*[51]⁵ and *DrQv2*[57]⁶ we use the official implementations provided by the respective authors.

DrQ(I+P) builds on the official implementation and uses a separate encoder for the proprioception whose output is concatenated to the image encoders' output and trained using the critics' gradients.

Differences between Model-Based *Img-Only(R)* and *Dreamer-v1*[15]. *Img-Only(R)* differs from the original Dreamer (*Dreamer-v1*) [15] in using the KL-balancing introduced in [16] and in regularizing the value function towards its own exponential moving average, as introduced in [18]. See Appendix B for all our training details and hyperparameters.

There are considerable differences between the contrastive version of *Dreamer-v1*[15] and *Img-Only(CV)*, in particular regarding the exact form of the mutual information estimation and the use of image augmentations.

²<https://github.com/danijar/dreamerv2/blob/main/scores/dmc-vision-dreamerv2.json>

³<https://github.com/fdeng18/dreamer-pro>

⁴<https://github.com/kyonofx/tia/>

⁵https://github.com/facebookresearch/denoised_mdp

⁶<https://github.com/facebookresearch/drqv2>

Differences between Model-Free *Img-Only(CPC)*, *FC-Joint(CPC)* and [45]. The main difference is that [45] includes the critic’s gradients when updating the representation while in our setting no gradients flow from the actor or the critic to the representation. Additionally, we adapted some hyperparameters to match those of our other approaches. The results are based on our implementation, not the official implementation of [45].

Why TIA and DenoisedMDP Fail in Our Setting. Both TIA [10] and DenoisedMDP [51] fail to perform well in the natural video background setting used in this work and [7], described in Section A.1. Both approaches factorize the latent variable into 2 distinct parts and formulate loss functions that force one part to focus on task-relevant aspects and the other on task-irrelevant aspects. However, the part responsible for the task-irrelevant aspects still has to model those explicitly. Recall the differences in adding the natural video backgrounds described in Appendix A. In this more complicated setting with randomly sampled, colored background videos, the TIA and DenoisedMDP world models underfit and thus fail to learn a good representation or policy. Contrastive approaches, such as our approach and DreamerPro [7], do not struggle with this issue, as they do not have to model task-irrelevant aspects but can learn to ignore them.

B Training and Architecture Details

We used the same hyperparameters in all experiments with the exception of the Box Pushing. For this task, we increased the number of free nats for the state space representation (see below) from 1 to 3.

B.1 Recurrent State Space Model

We denote the deterministic part of the *RSSM*’s state by \mathbf{h}_t and the stochastic part by \mathbf{s}_t . The base-*RSSM* model without parts specific to one of the objectives consists of:

- **Encoders:** $\psi_{\text{obs}}^{(k)}(\mathbf{o}_t)$, where ψ_{obs} is the convolutional architecture proposed by [12] and used by [14, 15] for image observations and a 3×400 Units fully connected NN with ELU activation for proprioceptive observations (, i.e., vectors).
- **Deterministic Path:** $\mathbf{h}_t = g(\mathbf{z}_{t-1}, \mathbf{a}_{t-1}, \mathbf{h}_{t-1}) = \text{GRU}(\psi_{\text{det}}(\mathbf{z}_{t-1}, \mathbf{a}_{t-1}), \mathbf{h}_{t-1})$ [6], where ψ_{det} is 2×400 units fully connected NN with ELU activation and the GRU has a memory size of 200.
- **Dynamics Model:** $p(\mathbf{z}_{t+1}|\mathbf{z}_t, \mathbf{a}_t) = \psi_{\text{dyn}}(\mathbf{h}_t)$, where ψ_{dyn} is a 2×400 units fully connected NN with ELU activation. The network learns the mean and standard deviation of the distribution.
- **Variational Distribution** $q(\mathbf{z}_t|\mathbf{z}_{t-1}, \mathbf{a}_{t-1}, \mathbf{o}_t) = \psi_{\text{var}}\left(\mathbf{h}_t, \text{Concat}\left(\{\psi_{\text{obs}}^{(k)}(\mathbf{o}_t^{(k)})\}_{k=1:K}\right)\right)$, where ψ_{var} is a 2×400 units fully connected NN with ELU activation. The network learns the mean and standard deviation of the distribution.
- **Reward Predictor** $p(r_t|\mathbf{z}_t)$: 2×128 units fully connected NN with ELU activation for model-free agents. 3×300 units fully connected NN with ELU activation for model-based agents. The network only learns the mean of the distribution. The standard deviation is fixed at 1. The model-based agents use a larger reward predictor as they rely on it for learning the policy and the value function. Model-free agents use the reward predictor only for representation learning and work with the ground truth rewards from the replay buffer to learn the critic.

B.2 Objectives

Image Inputs and Preprocessing. For the reconstruction objective, we used images of size 64×64 pixels as input to the model. For the contrastive objectives, the images are of size 76×76 pixel image and we used 64×64 pixel random crops. Cropping is temporally consistent, i.e., we used the same crop for all time steps in a sub-sequence. For evaluation, we took the crop from the center.

Reconstruction Objectives. Whenever we reconstructed images we used the up-convolutional architecture proposed by [12] and used by [14, 15]. For low-dimensional observations, we used 3×400 units fully connected NN with ELU activation. In all cases, only the mean is learned and the standard deviation is fixed at 1.

Table 3: Hyperparameters used for policy learning with the Soft Actor-Critic.

Hyperparameter	Value
Actor Hidden Layers	$3 \times 1,024$ Units
Actor Activation	ELU
Critic Hidden Layers	$3 \times 1,024$ Units
Critic Activation	ELU
Discount	0.99
Actor Learning Rate	0.001
Actor Gradient Clip Norm	10
Critic Learning Rate	0.001
Critic Gradient Clip Norm	100
Target Critic Decay	0.995
Target Critic Update Interval	1
α learning rate	0.001
initial α	0.1
target entropy	- action dim

For the KL terms in Equation 1 and Equation 3 we follow [18] and combine the KL-Balancing technique introduced in [16] with the *free-nats regularization* used in [14, 15]. Following [16] we use a balancing factor of 0.8. We give the algorithm 1 free nat for the DeepMind Control Suite and the Locomotion Suite tasks and 3 for the Box Pushing.

Contrastive Variational Objective. The score function for the contrastive variational objective is given as

$$f_v^{(k)}(\mathbf{o}_t^{(k)}, \mathbf{z}_t) = \exp\left(\frac{1}{\lambda} \rho_o\left(\psi_{\text{obs}}^{(k)}(\mathbf{o}_t)\right)^T \rho_z(\mathbf{z}_t)\right),$$

where $\psi_{\text{obs}}^{(k)}$ is the *RSSM*'s encoder and λ is a learnable inverse temperature parameter. ρ_o and ρ_z are projections that project the embedded observation and latent state to the same dimension, i.e., 50. ρ_o is only a single linear layer while ρ_z is a 2×256 fully connected NN with ELU activation. Both use LayerNorm [2] at the output.

Contrastive Predictive Objective. The score function of the contrastive predictive objective looks similar to the one of the contrastive variational objective. The only difference is that the latent state is forwarded in time using the *RSSM*'s transition model to account for the predictive nature of the objective,

$$f_p^{(k)}(\mathbf{o}_{t+1}^{(k)}, \mathbf{z}_t) = \exp\left(\frac{1}{\lambda} \rho_o\left(\psi_{\text{obs}}^{(k)}(\mathbf{o}_{t+1})\right)^T \rho_z(\phi_{\text{dyn}}(g(\mathbf{z}_t, \cdot)))\right).$$

We use the same projections as in the contrastive variational case.

Following [45] we scale the KL term using a factor of $\beta = 0.001$ and parameterize the inverse dynamics predictor as a 2×128 unit fully connected NN with ELU activations.

Optimizer. We used Adam [21] with $\alpha = 3 \times 10^{-4}$, $\beta_1 = 0.99$, $\beta_2 = 0.9$ and $\varepsilon = 10^{-8}$ for all losses. We clip gradients if the norm exceeds 10.

B.3 Soft Actor Critic

Table 3 lists the hyperparameters used for model-free RL with SAC [13].

We collected 5 initial sequences at random. During training, we update the *RSSM*, critic, and actor in an alternating fashion for d steps before collecting a new sequence by directly sampling from the maximum entropy policy. Here, d is set to be half of the environment steps collected per sequence (after accounting for potential action repeats). Each step uses 32 subsequences of length 32, uniformly sampled from all prior experience.

Table 4: Hyperparameters used for policy learning with *Latent Imagination*.

Hyperparameter	Value
Actor Hidden Layers	3×300 Units
Actor Activation	ELU
Critic Hidden Layers	3×300 Units
Critic Activation	ELU
Discount	0.99
Actor Learning Rate	8×10^{-5}
Actor Gradient Clip Norm	100
Value Function Learning Rate	8×10^{-5}
Value Gradient Clip Norm	100
Slow Value Decay	0.98
Slow Value Update Interval	1
Slow Value Regularizer	1
Imagination Horizon	15
Return lambda	0.95

B.4 Latent Imagination

Table 4 lists the hyperparameters used for model-based RL with latent imagination. They follow to a large extent those used in [15, 16].

We collected 5 initial sequences at random. During training, we update the *RSSM*, value function, and actor in an alternating fashion for 100 steps before collecting a new sequence. Each step uses 50 subsequences of length 50, uniformly sampled from all prior experience. For collecting new data, we use constant Gaussian exploration noise with $\sigma = 0.3$.

B.5 Compute Resources

Training a single agent takes between 8 and 12 hours on a single GPU (Nvidia V100 or A100), depending on which representation learning approach and RL paradigm we use. Approaches using a contrastive loss for the image are slightly faster than those that reconstruct the image as they do not have to run the relatively large up-convolutional image decoder. The model-free agents train slightly faster than the model-based ones, as the model-based ones have to predict several steps into the future for latent imagination. Especially propagating gradient back through this unrolling is relatively costly compared to a SAC update. Including all baselines, we trained about 3,500 agents for the final evaluation. Also including preliminary experiments, we estimate the total compute resources invested in this work to be about 50,000 GPU hours.

C Complete Results

C.1 Model-Free Agents

Here we list the aggregated results for all methods with model-free agents on the DeepMind Control (DMC) Suite with standard images (Figure 7), natural video background (Figure 8), and occlusions (Figure 9).

C.2 Model-Based Agents

Here we list the aggregated results for all methods with model-based agents on the DeepMind Control (DMC) Suite with standard images (Figure 10), natural video background (Figure 11), and occlusions (Figure 12).

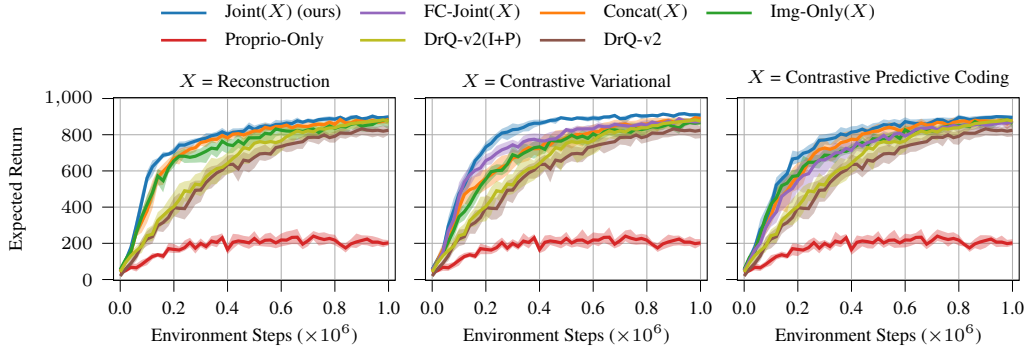


Figure 7: Aggregated results for **model-free** agents on the DMC Suite tasks with standard images. (*Img-Only(R)*) achieves similar performance to the model-free *DrQ-v2*, but also to *Dreamer-v2* and *DreamerPro* (see Figure 10), showing that our general representation learning approach also works without multiple sensors. However, using both images and proprioception is still advantageous in these tasks, and using joint representations leads to larger performance gains.

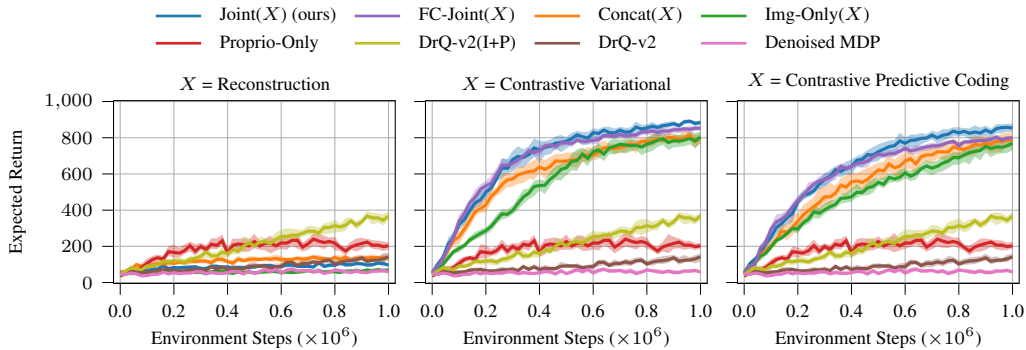


Figure 8: Aggregated results for **model-free** agents on the DMC Suite tasks with natural video background. As expected, all purely reconstruction-based approaches fail at the task, while those using a contrastive loss for the images achieve better results. The results are consistent between contrastive variational and predictive coding approaches. For both *Concat(X)* only improves the sample efficiency while joint representation learning can also increase the final performance. Using a contrastive image loss in combination with reconstruction for proprioception gives the best results.

C.3 Results per Environment - Model Free

The following figures provide the per environment results for model-free agents on the DMC Suite with standard images (Figure 13), model-free agents on the DMC Suite with natural video background (Figure 14), model-free agents on the DMC Suite with occlusion (Figure 15), model-based agents on the DMC Suite with standard images (Figure 16), model-based agents on the DMC Suite with natural video background (Figure 17), model-based agents on the DMC Suite with occlusion (Figure 17), and for the Locomotion Suite (Figure 19). We again report interquartile means and 95% bootstrapped confidence intervals [1].

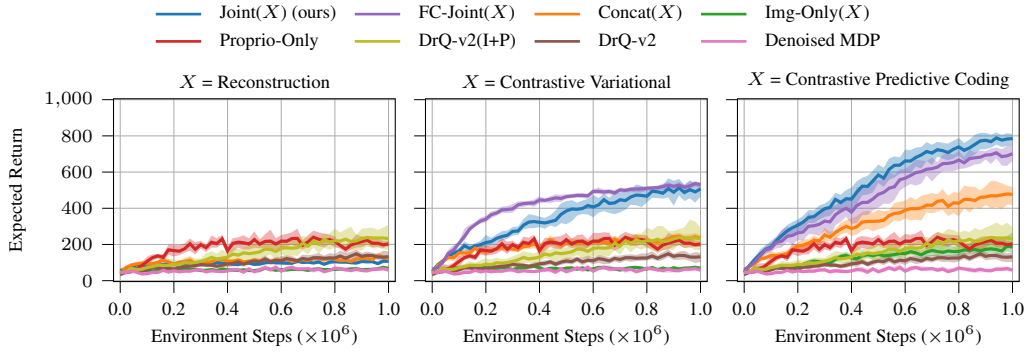


Figure 9: Aggregated results for **model-free** agents on the DMC Suite tasks with occlusion. In this task, no method that uses only images or reconstructs images performs better than solely using proprioception. However, combining both modalities and using contrastive methods for the images leads to vast performance improvements. While, at least for contrastive predictive coding, these improvements are already significant for the concatenation approach, joint representation learning gives even more performance. In this task, the contrastive predictive coding methods outperform contrastive variational ones arguably because their explicit ahead prediction allows them to learn better dynamics.

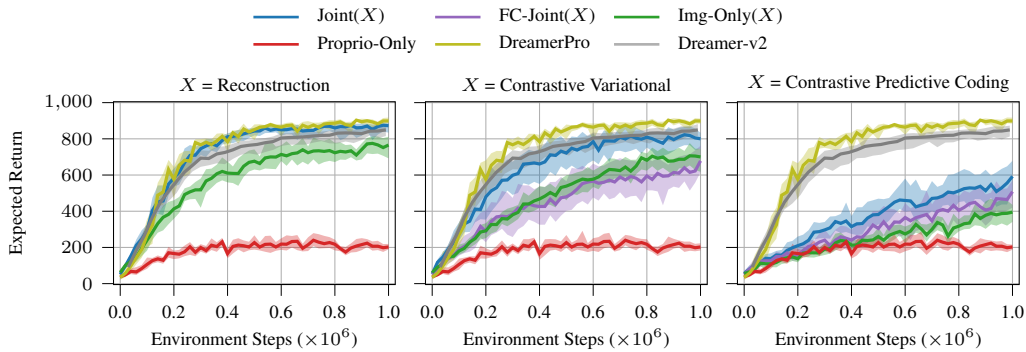


Figure 10: Aggregated results for **model-based** agents on the DMC Suite tasks with standard images. Unsurprisingly all reconstruction-based approaches obtain good performance. Notably, contrastive variational approaches perform better than constructive predictive ones with model-based agents, while they perform equally well with model-free agents. However, in both cases, a combination of contrastive and reconstruction-based losses outperforms the purely contrastive approaches.

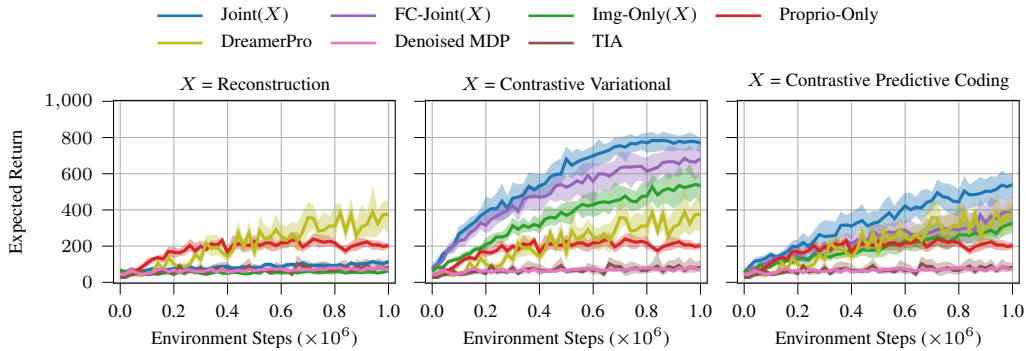


Figure 11: Aggregated results for **model-based** agents on the DMC Suite Tasks with natural video background. Again, all reconstruction-based approaches predictably fail. Furthermore, the contrastive variational approach again seems more suited for model-based agents than the contrastive predictive one, and the combination of contrastive and reconstruction-based losses performs best.

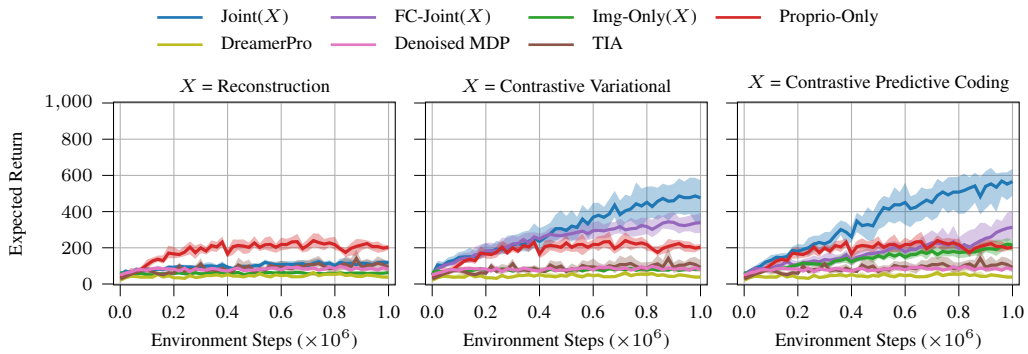


Figure 12: Aggregated results for **model-based** agents on the DMC Suite Tasks with occlusions. *Joint(CPC)* performs best among all approaches and almost achieves the same performance as on the simpler tasks with the standard images and natural video background. However, model-based *Joint(CPC)* is still significantly worse than its model-free counterpart.

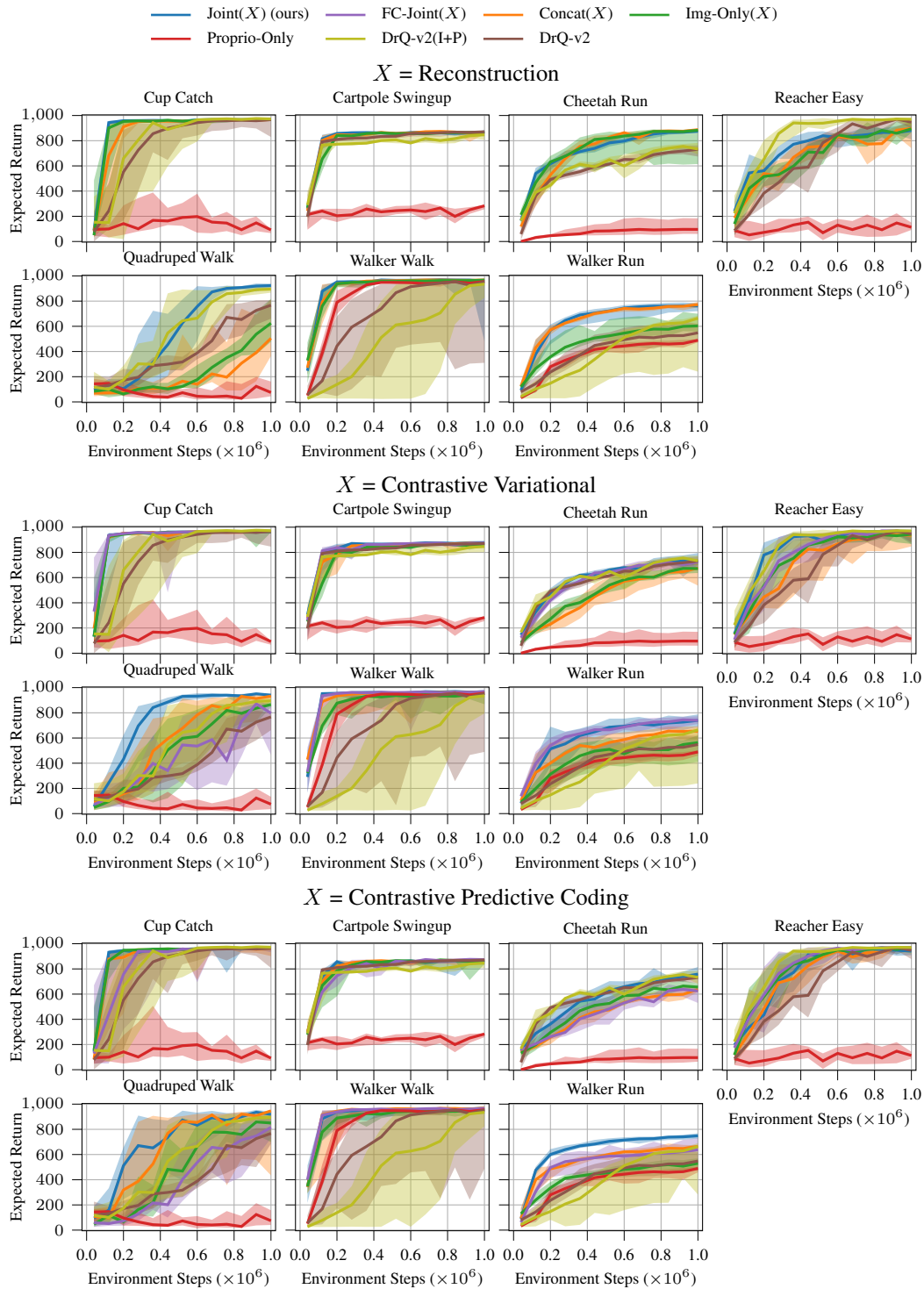


Figure 13: Per environment results for **model-free** agents on the DMC Suite with standard images.

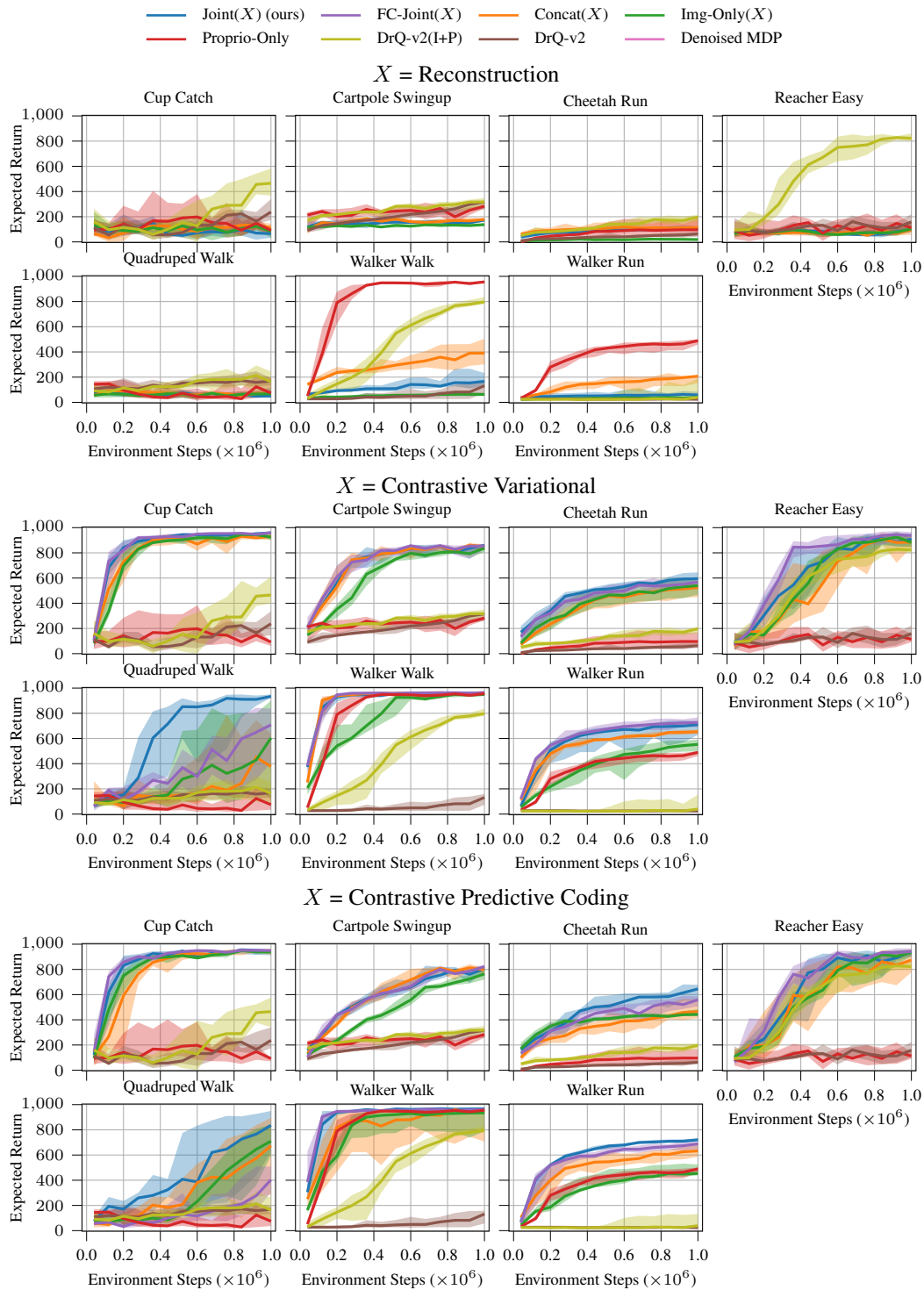


Figure 14: Per environment results for **model-free** agents on the DMC Suite with natural image background.

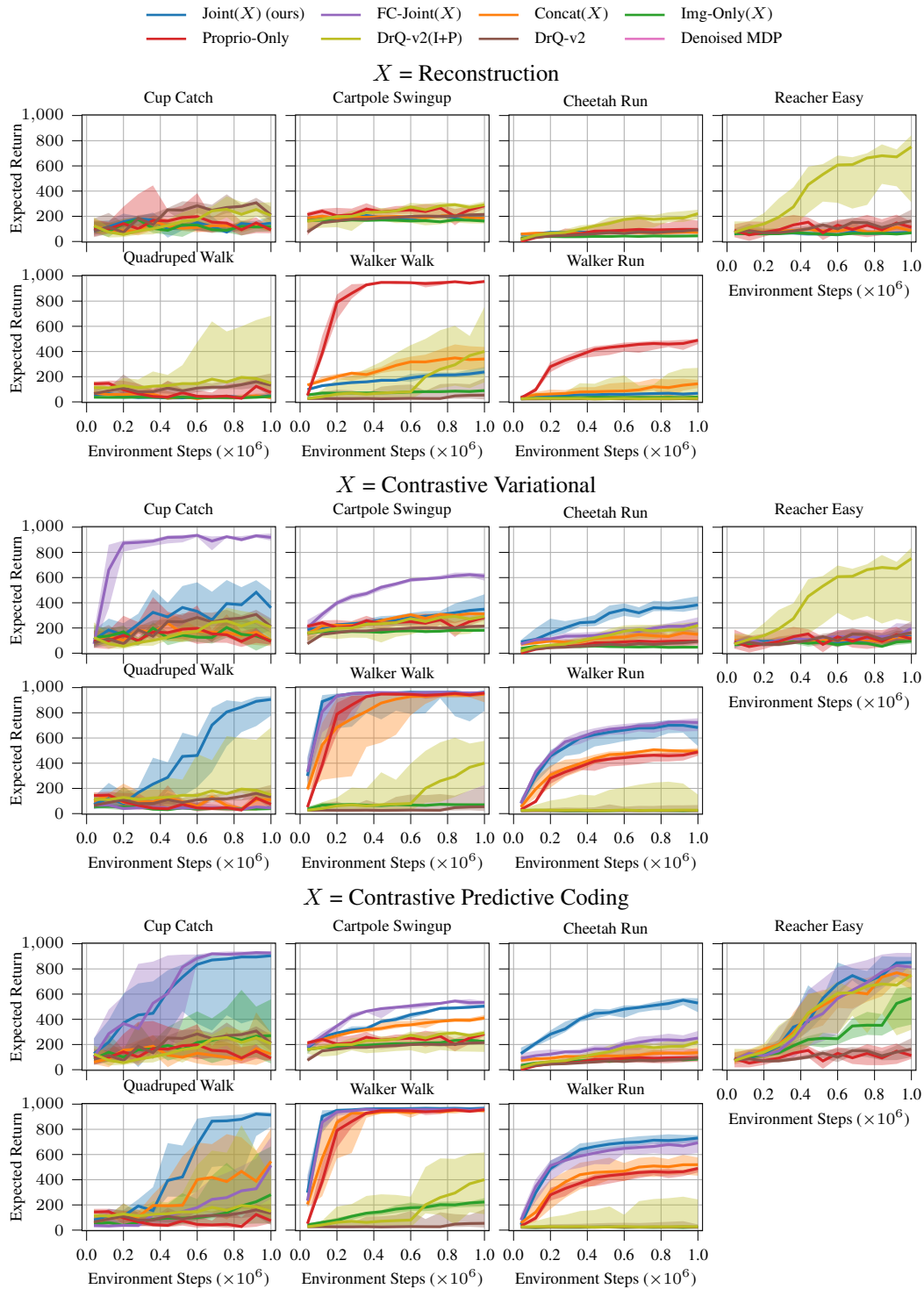


Figure 15: Per environment results for **model-free** agents on the DMC Suite with occlusion.

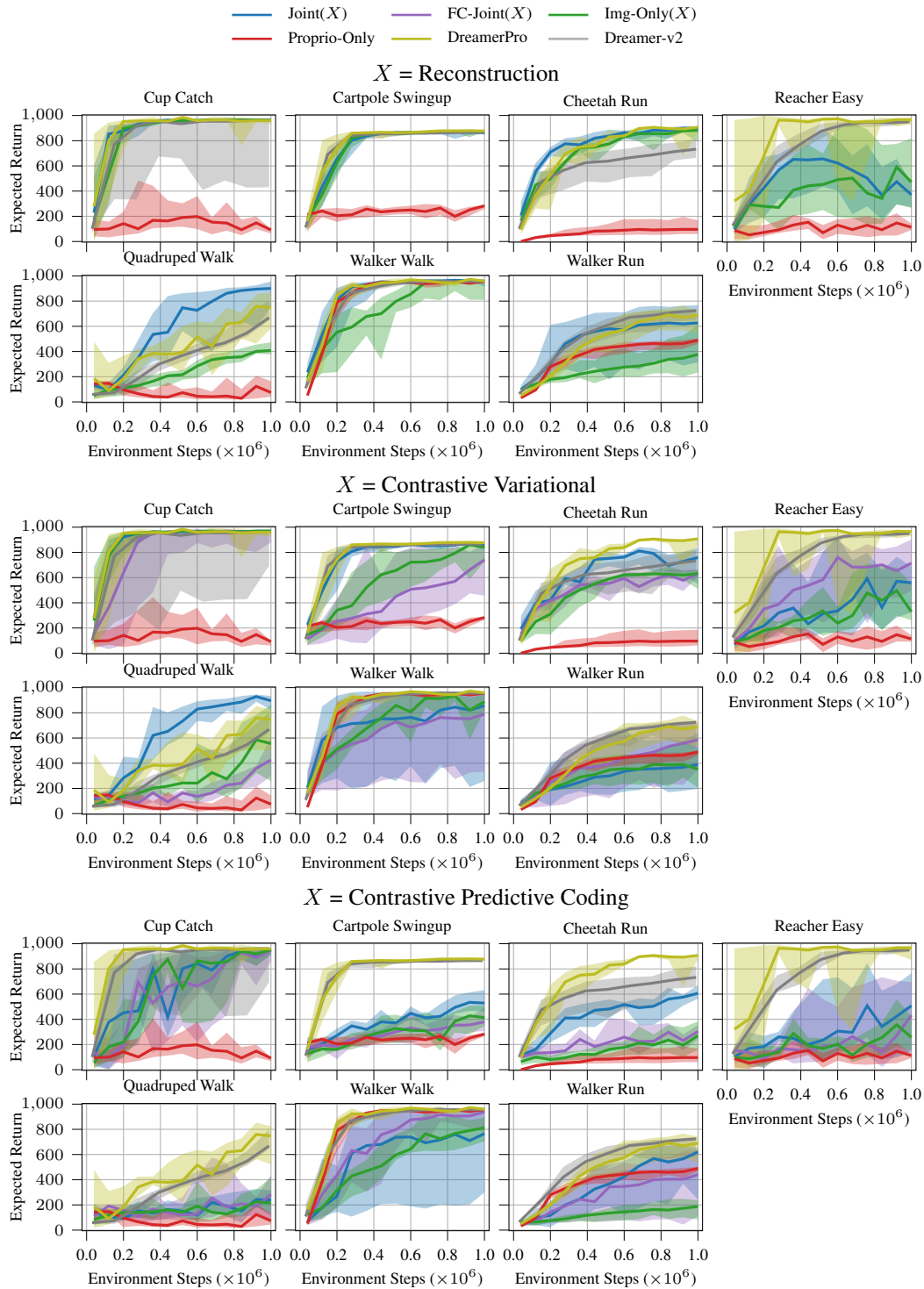


Figure 16: Per environment results for **model-based** agents on the DMC Suite with standard images.

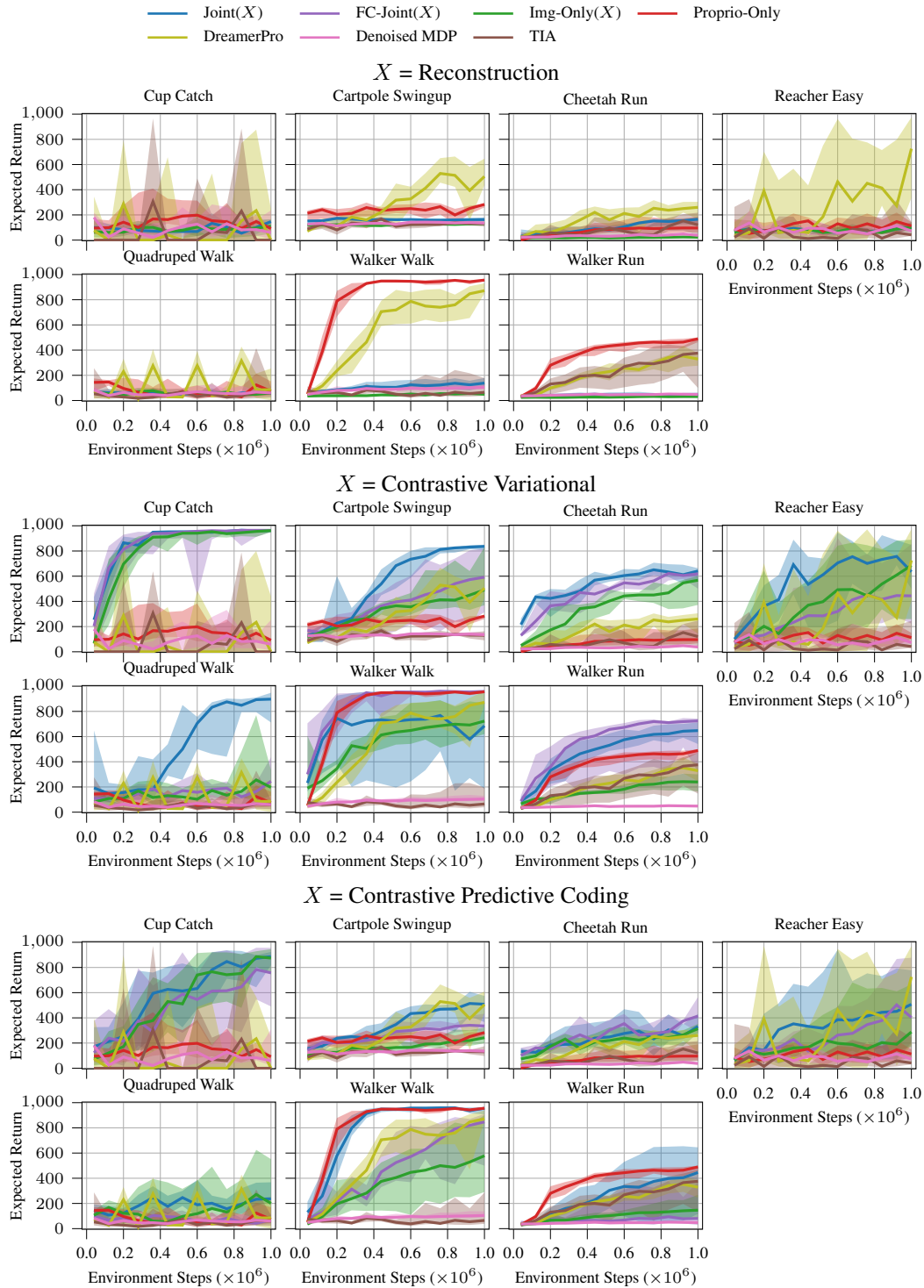


Figure 17: Per environment results for **model-based** agents on the DMC Suite with natural video background.

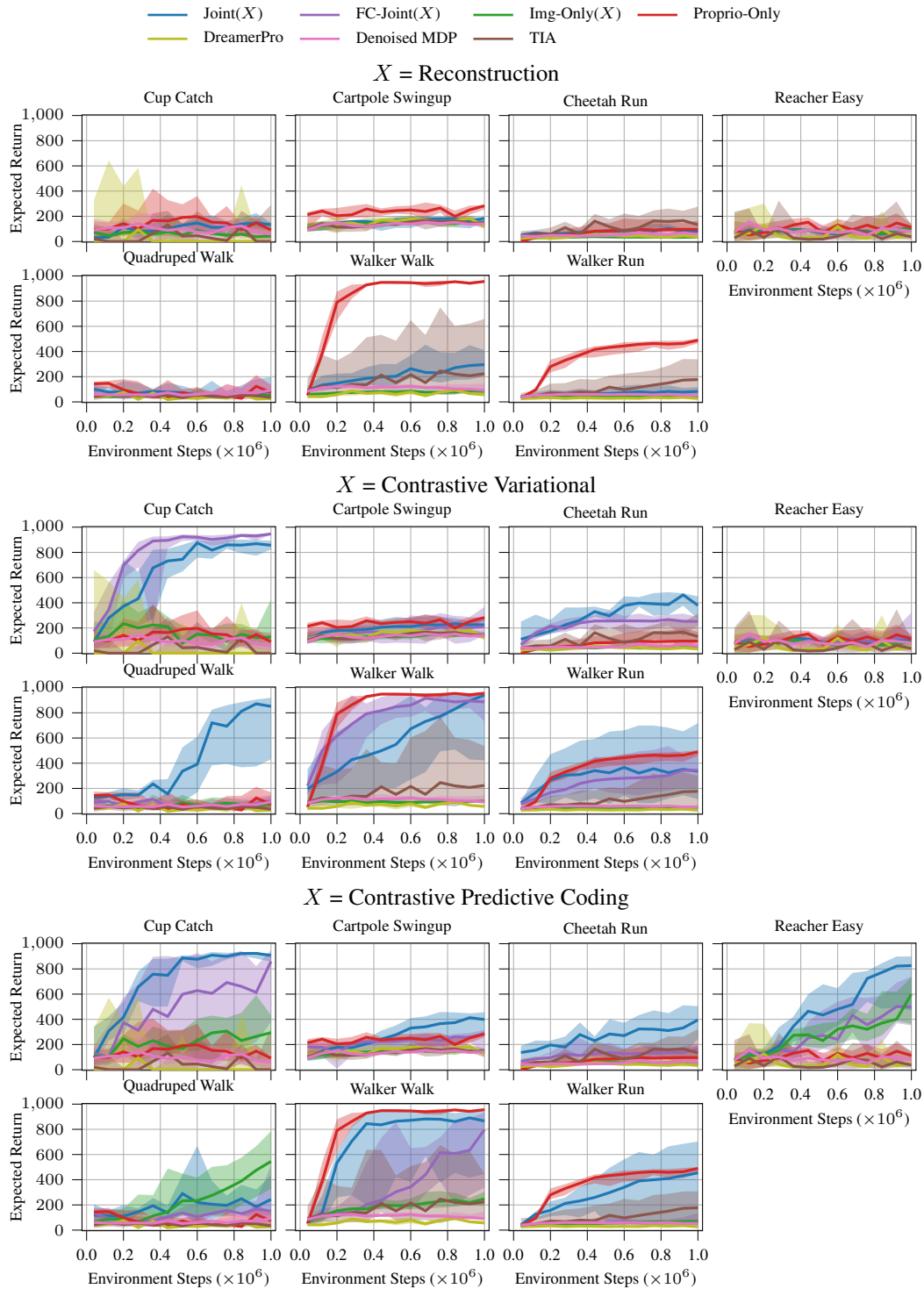


Figure 18: Per environment results for **model-based** agents on the DMC Suite with occlusions.

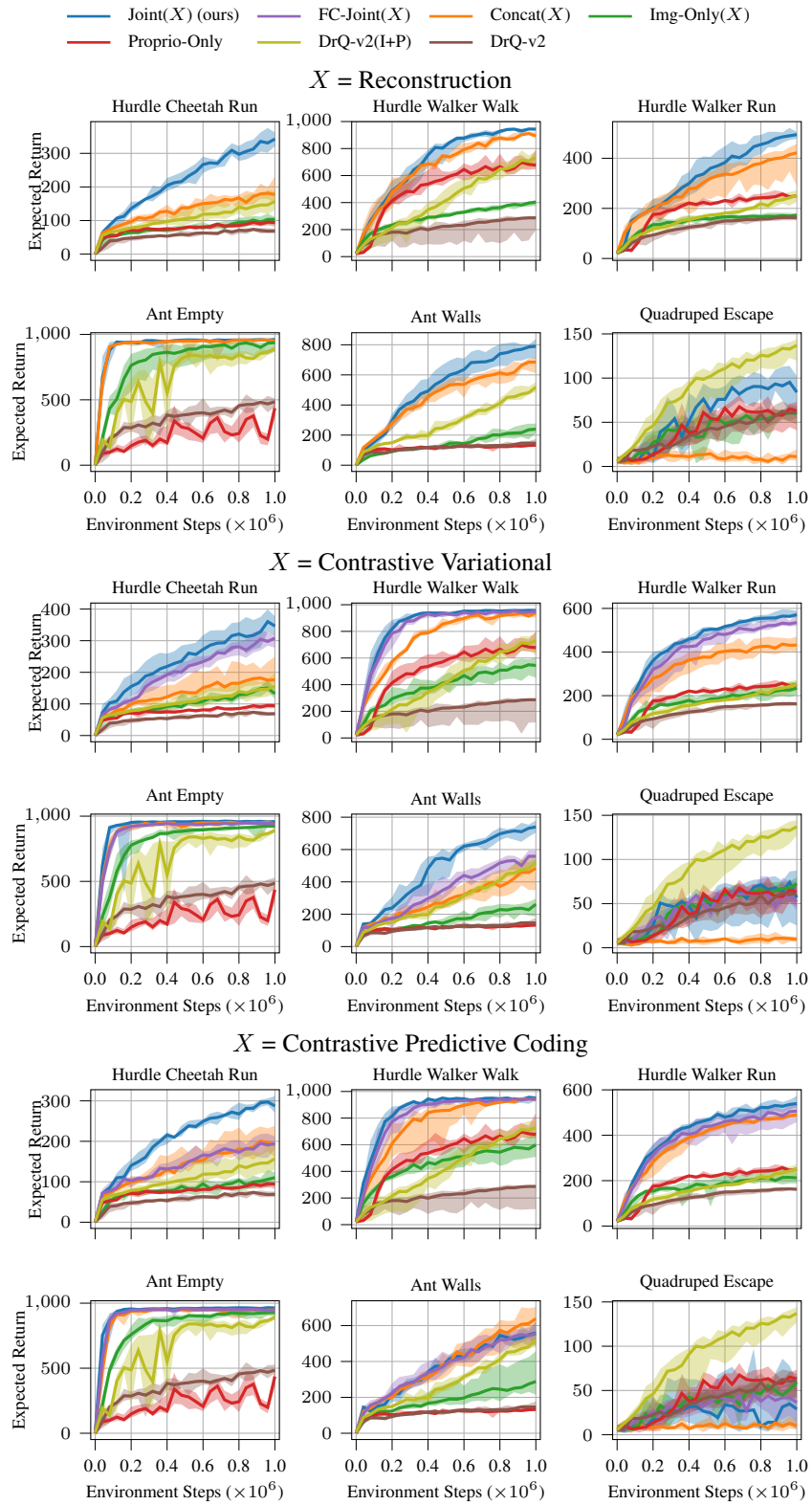


Figure 19: Per environment results for **model-free** agents on the Locomotion Suite.